Nanoscale

PAPER

View Article Online
View Journal | View Issue

Cite this: *Nanoscale*, 2016, **8**, 10598

Thermal exfoliation of stoichiometric single-layer silica from the stishovite phase: insight from first-principles calculations†

Yaguang Guo,[a,b] Shunhong Zhang,[a,b] Tianshan Zhao[a,b] and Qian Wang*[a,b]

Received 1st October 2015,
Accepted 17th December 2015

DOI: 10.1039/c5nr06788j

www.rsc.org/nanoscale

Mechanical cleavage, chemical intercalation and chemical vapor deposition are the main methods that are currently used to synthesize nanosheets or monolayers. Here, we propose a new strategy, thermal exfoliation for the fabrication of silica monolayers. Using a variety of state-of-the-art theoretical calculations we show that a stoichiometric single-layer silica with a tetragonal lattice, T-silica, can be thermally exfoliated from the stishovite phase in a clean environment at room temperature. The resulting single-layer silica is dynamically, thermally, and mechanically stable with exceptional properties, including a large band gap of 7.2 eV, an unusual negative Poisson's ratio, a giant Stark effect, and a high breakdown voltage. Moreover, other analogous structures like single-layer GeO_2 can also be obtained by thermal exfoliation of its bulk phase. Our findings are expected to motivate experimental efforts on developing new techniques for the synthesis of monolayer materials.

Introduction

Silicon and its derivatives have attracted tremendous attention due to their compatibility with the well-developed Si-based semiconductor industry. The discovery of silicene and its novel physical properties[1,2] has led to considerable interest in exploring other low dimensional Si-based nanomaterials. Among these, silica (SiO_2), one of the most abundant and complex inorganic compounds on earth, has been widely and intensively studied. Its two-dimensional (2D) form has recently drawn a lot of attention. Many efforts have been made to synthesize silica thin films. In particular, substantial progress has been achieved in the fabrication of hexagonal bilayer silica (HBS) through surface growth on Ru (0001)[3–5] or graphene.[6] Besides the bilayer structure, discovering single-layer silica sheets has also become a hot topic, and several 2D non-stoichiometric silica structures have been synthesized or predicted in the past few years. For instance, silicatene with a $SiO_{2.5}$ stoichiometry was grown on Mo (112)[7,8] and a single-layer honeycomb-like network hα (Si_2O_3) was predicted from first-principles calculations.[9]

Previous work has demonstrated that most silica polymorphs with a rigorous stoichiometry of Si : O = 1 : 2 have a strong ionic character, and can be viewed as $Si^{4+}(O^{2-})_2$.[10] Such an ionic character in covalent compounds is beneficial to the phase stability against amorphization or disproportionation. Very recently, the Pandey group[11] predicated a stoichiometric single-layer SiO_2 sheet with a tetrahedral configuration (named as T-silica) using a particle swarm optimization technique and first-principles calculations. They found that T-silica is insulating but becomes metallic when forming nanoribbons, implying its potential application to integrated circuits as a dielectric and/or conducting material. However, such a novel single-layer sheet has not yet been experimentally synthesized. One possible way might be the oxidation of silicene.[9] But the oxidation process is technically complex, and usually leads to different topological defects.[6,12] Therefore, it is highly desirable to develop new approaches rather than using surface growth or silicene oxidation for synthesizing such single-layer silica sheets.

In this paper, instead of silicene, we begin our study with stishovite, a bulk silica phase with a rutile-type structure, which has received great attention in high pressure physics, geochemistry, and materials science due to its novel hypervalency (six-fold coordinated silicon and 3-fold coordinated oxygen), ultrahigh density, and superhardness.[13] Different from previously studied pressure-induced "post-stishovite" polymorphs,[14–16] here special attention is paid to the nanostructured stishovite. Based on first-principles calculations, we demonstrate that thermal exfoliation is a possible way to fabricate silica monolayers from stishovite nanofilms. The resulting

[a]*Center for Applied Physics and Technology, College of Engineering, Peking University, Key Laboratory of High Energy Density Physics Simulation, and IFSA Collaborative Innovation Center, Ministry of Education, Beijing 100871, China. E-mail: qianwang2@pku.edu.cn*

[b]*Department of Materials Science and Engineering, College of Engineering, Peking University, Beijing 100871, China*

†Electronic supplementary information (ESI) available. See DOI: 10.1039/c5nr06788j

single-layer sheet exhibits unusual mechanical and electronic properties that are distinctly different from other previously studied layered silica structures.

Computational methods

First-principles calculations based on density functional theory (DFT) are carried out. The electronic exchange–correlation interaction is treated using the PBE functional within a generalized gradient approximation (GGA).[17] An all-electron Projector Augmented Wave (PAW) method implemented in the Vienna Ab initio Simulation Package (VASP)[18] is applied to study the ground state structure, electronic and mechanical properties of the new single layer silica. A hybrid functional in the Heyd–Scuseria–Ernzerhof (HSE06)[19] form is used for higher accuracy of the electronic structure calculations. The energy cutoff is set at 500 eV. The convergence criteria for energy and force are set as 0.0001 eV and 0.01 eV $Å^{-1}$, respectively. The Brillouin zone is represented with 9 × 9 × 1 Monkhorst–Pack special *k*-point meshes.[20] The vacuum space in the direction perpendicular to the sheet is taken to be 15 Å, which is sufficient to avoid interactions between two neighboring layers. To study the dynamical stability, phonon calculations are performed using a density functional perturbation theory (DFPT) method as implemented in the Quantum ESPRESSO code.[21] The canonical (NVT) ensemble *ab initio* molecular dynamics (AIMD) simulations are performed to simulate the structure evolution of stishovite nanofilms and examine the thermal stability of the silica and GeO_2 monolayers with temperature controlled by using a Nosé heat bath scheme.[22] Infrared and second-order Raman spectra are calculated by using the Quantum ESPRESSO code.[21] Troullier–Martins Norm-conserving pseudopotential[23] is used to treat core electrons. The energy cutoff for plane wave basis is set at 100 Ry. The first Brillouin zone is represented by a 15 × 15 × 1 Monkhorst–Pack meshed *k*-point grid.[20]

Results and discussion

Formation of T-silica

Fig. 1a shows the crystal structure of stishovite, the rutile-structured silica polymorph with space group $P4_2/mnm$, where the Si atoms adopt an octahedral coordination while the O atoms are tri-coordinated, leading to a higher density as compared to most bulk phases of silica. We started our research by examining how the structural stability of the stishovite nanofilms varies with their thickness. We used index *n* to represent the number of the slab replicas along the [001] direction of stishovite. A stishovite nanofilm with a thickness of *n* is denoted as *n*-SNF. We first optimized the structure of 2-SNF. By carefully checking the relaxed atomic configuration, a dramatic structural transformation is observed. The nanofilm decomposes into two silica single layers, as shown in Fig. 1b. The formation energy of the monolayer stishovite nanofilm is only 5 meV per atom, implying that the T-silica sheet has comparable thermodynamic stability with that of the bulk stishovite phase. A systematic study of its structural properties and stability was carried out using total energy calculations, AIMD simulations and phonon calculations, respectively. Our results indicate that the single-layer silica possesses tetragonal symmetry (layer group no. 59, $P\bar{4}m2$) with a lattice constant of $a = b = 2.84$ Å. This structure is not only dynamically and thermally stable, but also identical to that of the very recently predicated T-silica.[11] Therefore, we also name it as T-silica. The computational details and results are given in Text S1 and Fig. S1 in the ESI.† Interestingly, we note that some non-layered materials can also be spontaneously graphitized in ultrathin films.[24]

Based on this finding, we wondered if the thicker nanofilms would also undergo a similar structural transformation. Therefore, geometry optimization and total energy calculations were carried out for the stishovite nanofilms with $n > 2$. We found, unlike 2-SNF, all the other nanofilms do not spontaneously transform to the layered structure after optimizing their geometries. The variation of the lattice constant and formation energy with respect to the slab thickness (n) is plotted in Fig. 1d. We see that the formation energy, which is defined as the energy difference per formula unit between the nanofilm and its bulk phase, decreases monotonically as the thickness increases. Such enhanced thermodynamic stability is also observed in semiconductor nanocrystals due to the size dependence of structural metastability.[25] According to a previous study,[26] a 2D free standing sheet generally has a formation energy less than 200 meV per atom, while those with a higher formation energy may need a certain substrate for stabilization. In Fig. 1d, 3-SNF has the highest formation energy of 230 meV per atom. However, for the stishovite nanofilms with $n > 3$, the formation energies are less than 200 meV per atom, implying that they can be stable in a free standing state at low temperature. We further calculated the phonon spectra of the nanofilms by taking 3- and 4-SNFs as examples (see Fig. S2†). We found that all the vibrational modes are real in their Brillouin zone, implying that the stishovite nanofilms are dynamically stable. We also performed AIMD simulation at 100 K, and found that both 3- and 4-SNFs retain their original geometries without any obvious structural distortions. Thus, stishovite nanofilms are stable at low temperatures.

During the relaxation of 2-SNF, the formation of the individual T-silica single layer releases silicon atoms from the hyper-coordination states and hence significantly reduces the interatomic strain, leading to the energetic preference as compared to the thicker *n*-SNF ($n > 2$). Therefore, it is reasonable to expect that the thicker stishovite nanofilms would undergo the structural transformation if sufficient activation energy is provided to surmount the kinetic energy barrier. To manifest this anticipation, we heated the 4-SNF sheet by performing the NVT ensemble AIMD simulations at a higher temperature of 300 K. We observed that the surface layers are progressively exfoliated from the nanofilm, as shown in Fig. 2a. After 400 femtoseconds (fs), the nanofilm completely decomposes into four individual T-silica layers, and afterwards the layered struc-

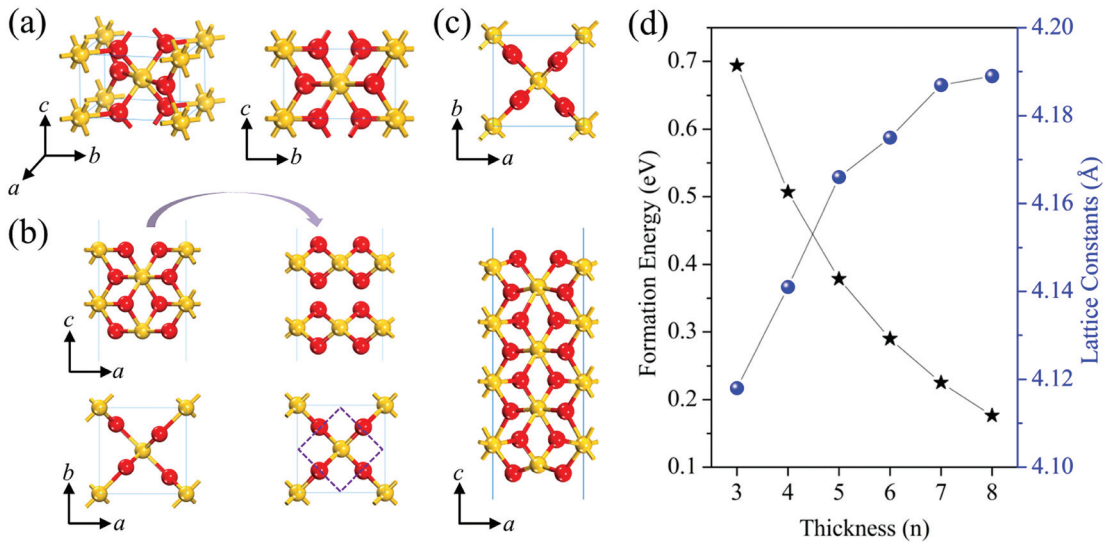

Fig. 1 Optimized crystal structure of (a) stishovite. (b) Left and right panels show the initial and optimized structures of 2-SNF. Purple dashed lines denote the unit cell. (c) Optimized structure of 4-SNF. (d) Variation of formation energy and lattice constant of *n*-SNF with thickness (*n*). Yellow and red balls represent silicon and oxygen atoms, respectively.

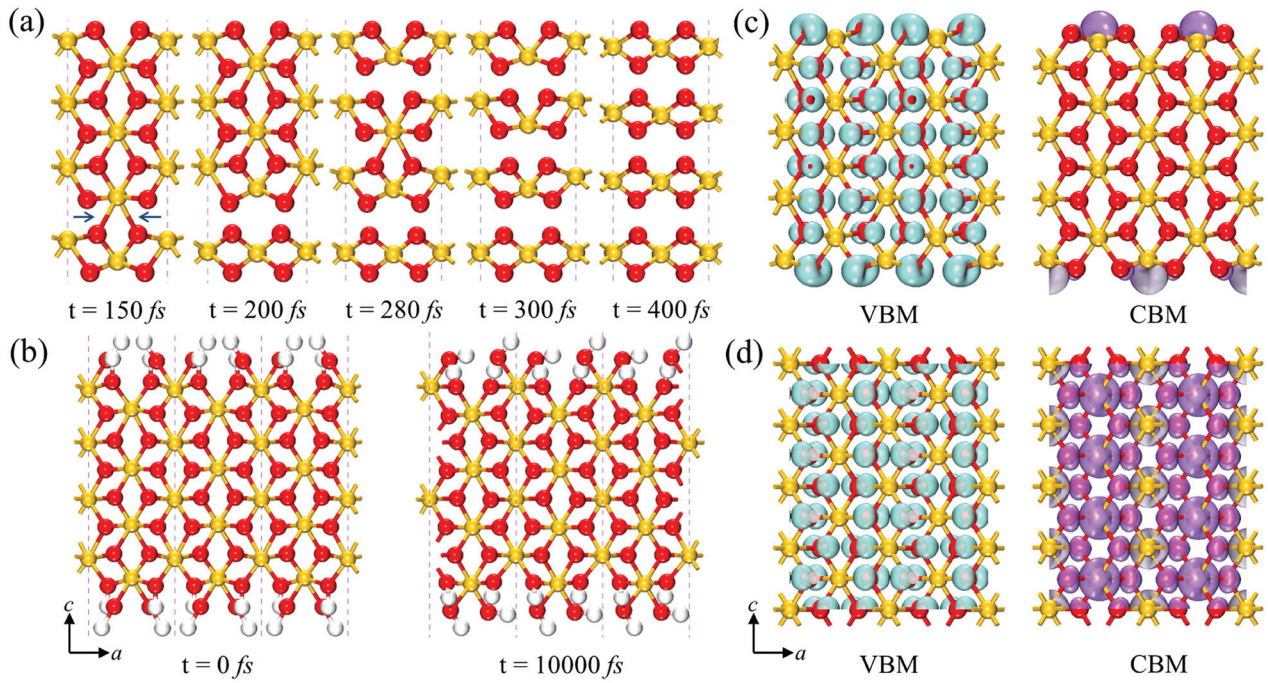

Fig. 2 Side view snapshots of (a) 4-SNF during the AIMD simulations at 300 K. (b) Snapshots of the surface-saturated 4-SNF at the beginning and end of the simulations at 300 K. The arrows in (a) indicate the stretched Si–O bonds that are broken when heated. (c) and (d) show the band-decomposed charge density of 4-SNF and bulk stishovite, respectively.

ture remains unchanged until the end of the simulation at 10 picoseconds (ps). We then performed simulated annealing from 300 K to 0 K, and the four T-silica layers are still detached, suggesting the phase transition is irreversible. To reduce the effect of the unit cell protected high symmetry on the thermal exfoliation and explore possible structure reconstruction, we performed AIMD simulation for a 3 × 3 supercell of the 4-SNF sheet by following the same procedure as described above. We found that the individual T-silica single layers can also be formed and no structure reconstruction occurs after reducing the constraint of periodic boundary conditions (see Fig. S3 in the ESI†). To take van der Waals (vdW)

interaction into consideration, we added the vdW correction (DFT-D2 in Grimme's formalism)[27] into AIMD simulations. The results show that after heating for 10 ps, the distance between the two T-silica layers enlarges to about 10 Å (see Fig. S3 in the ESI†), implying that the weak vdW interaction cannot prevent this thermal exfoliation process. Our simulation results indicate that, on the clean surfaces of stishovite, the T-silica sheet can be thermally exfoliated at room temperature. Such a growth process is technically simpler than the surface growth, hence is experimentally feasible.

We then explored the reason why stishovite nanofilms can transform into the layered structure. In general, the Si–O bond length is around 1.60–1.80 Å. However, when a nanofilm is cleaved from the bulk stishovite, some of the bonds are stretched to over 1.90 Å for strain release (indicated by arrows in Fig. 2a). Previous work has demonstrated that the longer (*i.e.*, the weaker) bonds are more prone to be further weakened upon excitation, which leads to a structural instability.[28] Based on this argument, the stretched bonds easily break up when the stishovite nanofilm is heated, as confirmed by our AIMD simulations. Fig. 2a shows that the T-silica layers are successively exfoliated from the surfaces of 4-SNF. The difference between the surface and interior atoms is that the surface Si atoms hold a four-fold coordination, resulting in a highly distorted Si–O tetrahedron, while the interior Si atoms have a six-fold coordination like those in the bulk stishovite. The formation of a slab *via* cleaving its bulk phase usually leads to a reduction in the coordination number of the surface atoms and charge redistribution. To visualize the changes, we calculated the charge density of the valence band maximum (VBM) and the conduction band minimum (CBM) for both 4-SNF and the bulk stishovite. The results are plotted in Fig. 2c and d, respectively. Comparing the two panels of Fig. 2c and d, we conclude that the thermal instability of 4-SNF is due to the charge redistribution at the surface of 4-SNF. In the bulk stishovite, each Si atom forms an octahedron with its neighboring O atoms, thus a uniform charge distribution is formed. While, in 4-SNF, the charge prefers to distribute on the Si atoms located at the outermost surface due to the surface relaxation, as shown in Fig. 2c. It was demonstrated that in nanofilms, surface contribution dominates the total energy.[24] Therefore, the formation energy of 4-SNF is relatively large (0.5 eV f.u.$^{-1}$) as shown in Fig. 1d. Thus, the T-silica sheet can be easily exfoliated from the nanofilms by the thermal treatment.

Based on the surface effect, it is understandable that the structural transformation may not occur if we terminate the surface atoms. In previous studies, several ways to stabilize the surface have been suggested,[29] like the adsorption of H adatoms.[30] Here, we use hydroxyls (OH) to saturate the Si atoms and H to saturate the O atoms on the surface of 4-SNF, as shown in Fig. 2b. In such circumstances the surface atoms are in a chemical environment similar to the interior atoms. As expected, throughout the AIMD simulations for 10 000 fs at 300 K, the geometry of the modified 4-SNF is nearly intact, implying that the surface modified 4-SNF is stable. Therefore, the thermal instability of the stishovite nanofilm comes from the unsaturated surface atoms. In other words, the T-silica layers only can be thermally exfoliated in a clean environment. Adatoms or radicals absorbed on the surface of the stishovite nanofilm enhances the stability of the nanofilms, consequently the T-silica layer cannot be exfoliated through the thermal treatment. Thus, a high vacuum environment is essential to thermally exfoliate the stishovite nanofilms to produce silica single layers in experiments.

It is now clear that the T-silica sheet can be thermally exfoliated at room temperature. Besides the aforementioned high vacuum environment and mild thermal treatment, the thickness of stishovite nanofilm is also a crucial factor for the exfoliation of T-silica. From Fig. 1d, we see that when $n > 3$, the formation energy decreases monotonically with the thickness, which means that the thermodynamic stability of the nanofilm is gradually enhanced. Accordingly, the difference in the electronic structure between the nanofilm and bulk stishovite reduces. The thicker the film is, the weaker the surface effect will be. Based on our calculations, we find that thermal exfoliation does not occur, when the thickness of n is more than seven. Thus, an ultrathin film is required to achieve the thermal exfoliation.

To aid experimentalists in the characterization of the T-silica structure, we calculated its infrared and second-order Raman spectra using the second-order response method.[31] The vibrational modes of T-silica at the Brillouin zone center are subject to D_{2d} symmetry, and the irreducible representations of the phonons at the Γ point can be expressed as:

$$\Gamma = 2\mathrm{B}_2(I+R) \oplus 3\mathrm{E}(I+R) \oplus \mathrm{A}_1(R). \quad (1)$$

The calculated infrared and Raman spectra of T-silica are plotted in Fig. 3. All optical modes at the Brillouin zone center have Raman activity while their intensity varies drastically

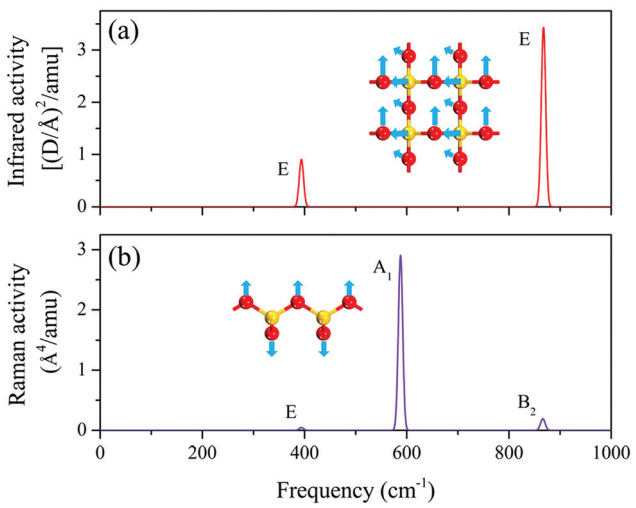

Fig. 3 Calculated vibrational (a) infrared and (b) Raman spectra of T-silica. The insets in (a) and (b) show the atomic vibration of the modes with the highest peak.

from one to another. We found that the out-of-plane vibration of oxygen atoms leads to a significant Raman peak at 588 cm^{-1} (with A_1 symmetry according to group theory). Such a characteristic peak signal can be used as a valuable clue to identify the T-silica phase in experiments.

The significant distinction between the silica phases under high-pressure and ambient pressure is the coordination number of Si atoms. In high-pressure silica phases, such as stishovite and seifertite, the Si atoms possess a six-fold coordination, forming Si–O octahedra. While in the phases at ambient pressure, like quartz and cristobalite, the silicon atoms prefer a four-fold coordination, forming Si–O tetrahedra. According to previous studies,[32] increasing the coordination number of Si atoms can be realized through compression of silica. The average coordination number of the Si atom has a positive correlation with external pressure. Although the T-silica phase is formed from the stishovite nanofilm, unlike stishovite which contains six-fold coordinated Si atoms, it only possesses four-fold coordinated Si atoms. Thus, T-silica is not a high-pressure phase and can exist under ambient conditions, which is also confirmed by our phonon calculations and AIMD simulations without external pressure.

The rutile-structured polymorph exists not only in bulk silica, but also in other dioxides of IVA group elements, such as GeO_2, SnO_2, and PbO_2. In fact, T-silica is a structural analog of our previously proposed graphene dioxide (GDO).[33] So we wonder if the T-silica structure is stable for GeO_2, SnO_2, and PbO_2, and if it is also possible to thermally exfoliate the layered structure from their bulk phases? We carried out similar calculations for GeO_2, SnO_2, and PbO_2. Our geometry optimizations and phonon calculations indicate that the T-silica structured single-layer GeO_2 (T-GeO_2) and SnO_2 (T-SnO_2) are dynamically stable, while PbO_2 cannot exist in such a single-layer structure. The thermal exfoliation of single-layer GeO_2 sheets can be achieved at 600 K from its bulk phase. The details of the formation of the T-GeO_2 sheet and the study on its structural and electronic properties, and stability are presented in Text S4, Fig. S4 and S5 in the ESI.† However, the SnO_2 nanofilms are still almost intact when the temperature of AIMD simulations is increased to the melting point of its bulk phase. So, we see that it is impossible to thermally exfoliate the T-SnO_2 sheet from its bulk phase.

So far, by elucidating the structural relationship between T-silica and the well-known high pressure stishovite phase, we have demonstrated the mechanism of thermal exfoliation of the monolayers, and suggested a viable strategy to fabricate T-silica. Next we explore the uncovered properties of this sheet for various future applications.

Mechanical properties

We first focus on the mechanical properties of the T-silica sheet. The elastic constants are calculated to be: $C_{11} = C_{22} = 169.7$ N m^{-1}, $C_{12} = -12.8$ N m^{-1}, and $C_{44} = 15.6$ N m^{-1}. They satisfy the Born–Huang criteria,[34] namely, $C_{11}C_{22} - {C_{12}}^2 > 0$ and $C_{44} > 0$, indicating that the T-silica sheet is mechanically stable. For some 2D structures like graphene, the in-plane stiffness has been well studied. Most currently synthesized 2D materials possess hexagonal symmetry and hence exhibit isotropic in-plane elastic properties. We calculated the Young's modulus and Poisson's ratio by using the following formulae:[35,36]

$$E(\theta) = \frac{C_{11}C_{22} - {C_{12}}^2}{C_{11}s^4 + C_{11}c^4 + \left(\frac{C_{11}C_{22} - {C_{12}}^2}{C_{44}} - 2C_{12}\right)c^2s^2}, \quad (2)$$

$$\nu(\theta) = -\frac{\left(C_{11} + C_{22} - \frac{C_{11}C_{22} - {C_{12}}^2}{C_{44}}\right)c^2s^2 - C_{12}(c^4 + s^4)}{C_{11}s^4 + C_{22}c^4 + \left(\frac{C_{11}C_{22} - {C_{12}}^2}{C_{44}} - 2C_{12}\right)c^2s^2}, \quad (3)$$

where $c = \cos\theta$, and $s = \sin\theta$, and θ is the polar angle relative to the x axis in Fig. 4.

To visualize the direction-dependence, we depicted the calculated Young's moduli and Poisson's ratios in the polar diagrams as shown in Fig. 4a and b. The tetragonal symmetry of T-silica leads to the anisotropic mechanical behaviors. The Young's modulus reaches the largest value of 169 N m^{-1} along the x and y directions, which is comparable to that of the HBS[11] and silicene monoxides,[37] but is much larger than that of the single-layer hα phase[9] due to its denser configuration. For an isotropic incompressible material, the maximum Poisson's ratio is 0.5. However, for the tetragonal T-silica, the Poisson's ratio exceeds 0.5 in some directions, implying shear deformation may be easier to occur in such directions compared to tensile strain. The small Young's moduli in these (diagonal) directions further confirm such speculations. Interestingly, we note that the C_{12} value is negative for this sheet, leading to a negative Poisson's ratio along the x and y directions, *viz.* $\nu = C_{12}/C_{11} = -0.075$ as shown in Fig. 4b, which means that when stretched in one direction, the T-silica sheet will expand in the one perpendicular to it. To further confirm the negative Poisson's ratio of T-silica, we calculated the lateral response in the y direction when the lattice endures a tensile strain of 5% in the x direction. As expected, we found that the equilibrium lattice constant in the y direction is expanded about 0.7%. Materials with negative Poisson's ratio, which are called metamaterials or auxetics in the science community, are rarely seen in nature. A negative Poisson's ratio in bulk silica with a α-cristobalite structure was discovered more than two decades ago.[38] Recently, a negative Poisson's ratio was also predicted to exist in few-atom-thick 2D compounds, such as phosphorene,[39] hα-silica,[9] and penta-graphene.[40] We note that T-silica and penta-graphene share some common structural characteristics: they both have a tetragonal lattice, and contain three atomic layers with the central layer composed of group IVA atoms adopting sp^3-hybridization. The existence of the four-fold coordinated Si atoms with sp^3-hybridized orbitals may be the main reason why T-silica has a negative Poisson's ratio as is the case with penta-graphene.

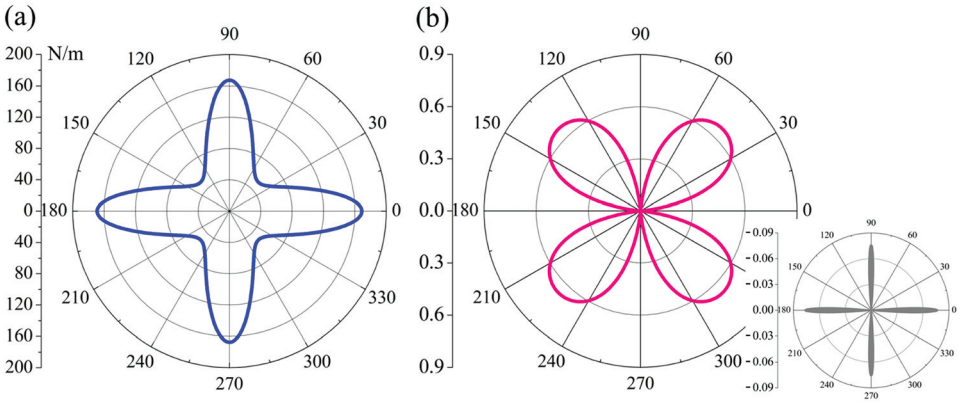

Fig. 4 Calculated (a) Young's modulus and (b) Poisson's ratio of T-silica. The inset shows the negative Poisson's ratio of T-silica along the axial directions.

Electronic properties

To study the electronic properties of the T-silica sheet, we calculated the electronic band structure and the band-decomposed charge density distribution corresponding to the VBM and CBM. The results are plotted in Fig. 5d and e, respectively, where no spin polarization is found, implying that T-silica is nonmagnetic. At the GGA/PBE level, T-silica is an indirect band gap insulator as the conduction band minimum (CBM) is located at the Γ point, while the valence band maximum (VBM) lies between the M and Γ point in the Brillouin zone. The calculated band gap is 5.40 eV, which is in good agreement with that of Pandey's work.[11] We then rectified the band gap using the more accurate HSE06 functional. Although the band dispersion is similar to that obtained at the GGA/PBE level, the band gap increases to 7.20 eV, which is very close to that of the HBS phase (7.19 eV), and much larger than that of any non-stoichiometric silica sheets,[9,37] demonstrating

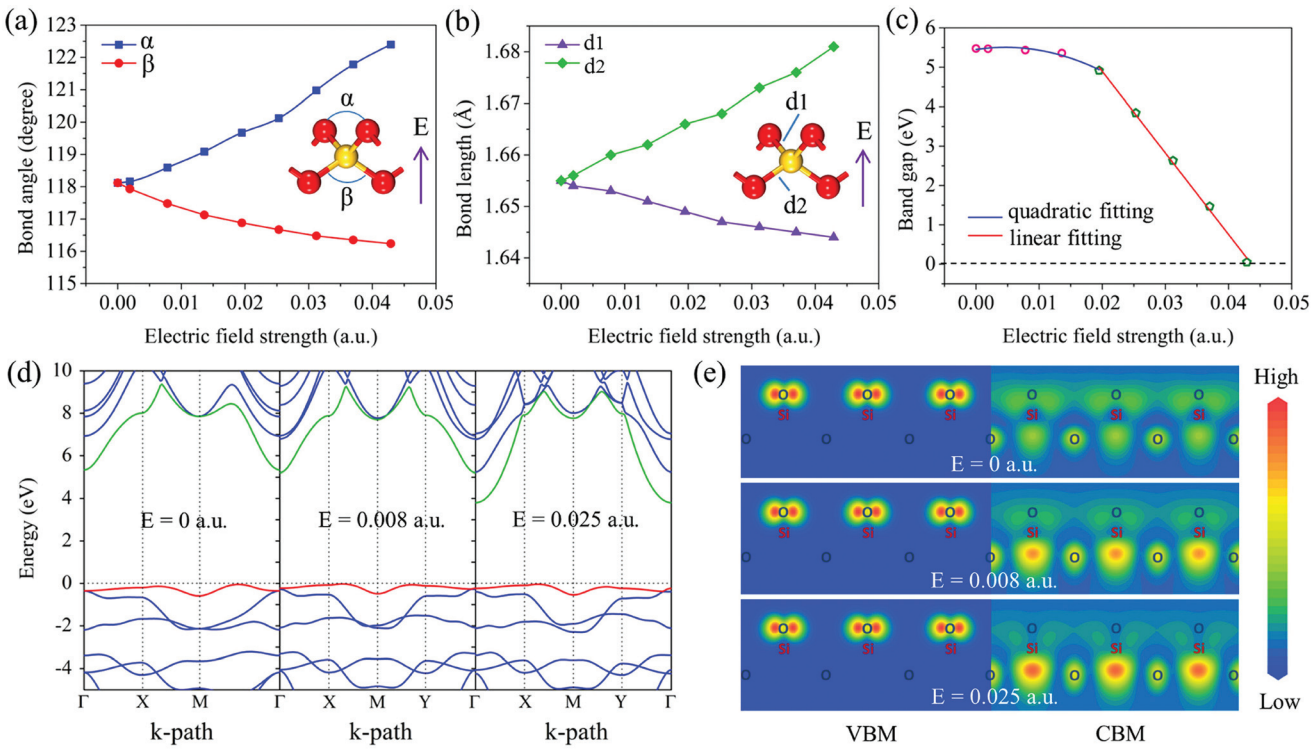

Fig. 5 Variation of (a) bond angles, (b) bond lengths, and (c) band gap with electronic field strength of T-silica. (d) Calculated band structures at the GGA/PBE level for different field strengths. (e) Charge density slices for the valence band maximum (VBM) and the conduction band minimum (CBM), corresponding to the red and green bands in (d), respectively.

that the oxidation level has a direct effect on the electronic structure. Comparing with the conventional insulators such as boron nitride and diamond, T-silica has an even larger band gap, and is more insulating. Thus it has potential application in electric capacitors, field effect transistors, or other electronic devices as a dielectric medium. The charge density distribution shows that the VBM is mainly contributed by the O 2p orbitals, whereas the CBM mainly comes from the Si 3s orbitals. The highest valence band is doubly degenerate at the Γ point due to the high symmetry of the tetragonal crystal system.

Band gap modulation by external electric field

The properties of insulators or semiconductors in an external electric field are very important not only from the fundamental point of view but also for practical applications as gate voltage is widely used in logic circuits. Therefore, we studied the effect of an electric field on the geometry and electronic properties of T-silica. We applied a uniform electric field along the non-periodic direction, namely the *z*-direction, and fully optimized the structure. For convenience of discussion, we define four parameters to describe the geometric change of T-silica: the bond angles, labeled as α and β, and the bond lengths, labeled as d_1 and d_2, as displayed in Fig. 5a and b. The figures show that α and d_2 increase, while β and d_1 decrease when the electric field strength is increased, leading to a structural distortion, and accordingly the structural symmetry degrades from $D_{2d}{}^5$ to $C_{2v}{}^1$. To investigate the underlying physical mechanism, we performed Bader charge analysis.[41] The calculated results show that in a unit cell, the silicon atom donates ~3.14 electrons, while each oxygen atom receives ~1.57 electrons. The transferred charge is much more than that in other 2D silica with different stoichiometries, such as hα-silica (Si_2O_3),[9] indicating that the Si–O bond has a strong ionic character. Due to the charge transfer, the Si atoms exhibit a cationic feature whereas the O atoms show an anionic feature, which results in a force along the electric field on the Si atoms, and a force against the field on the O atoms. Therefore, the Si atoms have an upward displacement while the O atoms move downwards upon the force, leading to the changes of the corresponding bond angles and bond lengths. A similar phenomenon was also observed in BN nanotubes under an electric field[42] because the charge transfers from B atoms to N atoms. Note that the structural deformation is not significant, and the structure recovers to its original shape when the electric field gradually decreases, implying that this geometric change can be considered as an elastic deformation.

The variation of the band gap of T-silica *versus* an external electric field is calculated at the GGA/PBE level, and is illustrated in Fig. 5c. We see that the band gap decreases quadratically when the field strength is small, while decreases linearly after a threshold field strength of about 0.020 a.u. is reached. Such a phenomenon has been reported and is called the Stark effect in previous studies,[42–45] which is analogous to the electric field induced spectral lines splitting in atomic physics. For a small electric field, according to Louie's work, the non-degenerate VBM and VBM lead to a quadratic reduction of the band gap.[42] However, when the field strength becomes substantially large, the field induced electrostatic potential is comparable to the band gap size, which gives rise to a linear field dependence.[46] To further understand the band gap reduction, we also calculated the band-decomposed charge density distribution for the CBM and VBM at the electric field of 0.008 and 0.025 a.u., respectively. The results are plotted in Fig. 5e, which shows that without the electric field, the charge density of the VBM is localized around the O atoms, whereas that of the CBM is distributed around the Si atoms. We see that when the electric field increases to 0.008 a.u., the VBM remains almost unchanged, while the charge density of the CBM dissipates in the direction opposite to the electric field, and accumulates under the Si atoms. The reason for the remarkable shift of charge density distribution of the CBM is because this state mainly comes from the Si 3s orbitals, which is weakly bonded and easily redistributed in response to the external field. On the contrary, the VBM mainly comes from the highly localized O 2p orbitals (electron lone pairs), thus showing a slight change in the electric field. The downshift of conduction band caused by the charge redistribution gives rise to the reduction of the band gap. In addition, the highest valence band, which exhibits a double degeneracy at the Γ point at a zero field, is split into two separate energy levels by about 0.15 eV as shown in Fig. 5d, due to the degraded symmetry caused by the lattice distortion. From Fig. 5c, we see that the energy gap is closed at the electric field of ~0.043 a.u., implying a breakdown of the insulating T-silica sheet. The geometric structure is still maintained in the breakdown state, and the process is reversible, which manifests that the breakdown for the T-silica sheet can be regarded as a soft breakdown.

Conclusions

In summary, we showed that T-silica, a tetragonal single layer of a stoichiometric silica sheet, can be obtained by thermally exfoliating stishovite nanofilms. We demonstrated that thermal exfoliation is a possible technique to fabricate silica and GeO_2 monolayers *via* a comprehensive first-principles DFT study of the structural relationship and phase transition between the single-layer structures and their bulk phases. We found that a spontaneous exfoliation of T-silica occurs for the ultrathin stishovite film with only two layers in a clean environment, while beyond this thickness, a finite temperature is needed to provide the activation energy for overcoming the kinetic energy barrier to induce the exfoliation. However, when the surface is saturated by some adatoms and radicals, such thermal exfoliation is prevented. Due to its special atomic configuration, T-silica has unusual properties that have not been uncovered yet, such as (1) it exhibits an anisotropic Young's modulus, different from the synthesized hexagonal bilayer silica; (2) it exhibits a negative Poisson's ratio, similar to that recently reported in single-layer hα-silica,[9] a black

phosphorus sheet,[39] and penta-graphene;[40] (3) it possesses a huge band gap of 7.20 eV (at the HSE06 level), even larger than that of conventional insulators like boron nitride and diamond; (4) it exhibits a large Stark effect and a high breakdown voltage. The exceptional properties exhibited in the studied layered structure extend its new potential applications to auxetic materials as well as good dielectric materials. Furthermore, our calculated infrared and second-order Raman spectra of T-silica provide a valuable reference for further experimental study. We hope that these findings will stimulate experimental interest in this field.

Acknowledgements

This work is partially supported by grants from the National Natural Science Foundation of China (NSFC-11174014 and NSFC-51471004), the National Grand Fundamental Research 973 Program of China (Grant No. 2012CB921404), and the Doctoral Program of Higher Education of China (20130001110033). The calculations were carried out at the Shanghai Supercomputer Center.

References

1 S. Cahangirov, M. Topsakal, E. Aktürk, H. Şahin and S. Ciraci, *Phys. Rev. Lett.*, 2009, **102**, 236804.
2 P. Vogt, P. De Padova, C. Quaresima, J. Avila, E. Frantzeskakis, M. C. Asensio, A. Resta, B. Ealet and G. Le Lay, *Phys. Rev. Lett.*, 2012, **108**, 155501.
3 D. Löffler, J. Uhlrich, M. Baron, B. Yang, X. Yu, L. Lichtenstein, L. Heinke, C. Büchner, M. Heyde and S. Shaikhutdinov, *Phys. Rev. Lett.*, 2010, **105**, 146104.
4 R. Włodarczyk, M. Sierka, J. Sauer, D. Löffler, J. Uhlrich, X. Yu, B. Yang, I. Groot, S. Shaikhutdinov and H.-J. Freund, *Phys. Rev. B: Condens. Matter*, 2012, **85**, 085403.
5 A. V. Krasheninnikov and F. Banhart, *ACS Nano*, 2013, **7**(6), 5175–5180.
6 P. Y. Huang, S. Kurasch, A. Srivastava, V. Skakalova, J. Kotakoski, A. V. Krasheninnikov, R. Hovden, Q. Mao, J. C. Meyer and J. Smet, *Nano Lett.*, 2012, **12**, 1081–1086.
7 J. Weissenrieder, S. Kaya, J.-L. Lu, H.-J. Gao, S. Shaikhutdinov, H.-J. Freund, M. Sierka, T. Todorova and J. Sauer, *Phys. Rev. Lett.*, 2005, **95**, 076103.
8 J. Seifert, D. Blauth and H. Winter, *Phys. Rev. Lett.*, 2009, **103**, 017601.
9 V. O. Özçelik, S. Cahangirov and S. Ciraci, *Phys. Rev. Lett.*, 2014, **112**, 246803.
10 K. AlKaabi, D. L. V. K. Prasad, P. Kroll, N. W. Ashcroft and R. Hoffmann, *J. Am. Chem. Soc.*, 2014, **136**, 3410–3423.
11 G. Wang, G. C. Loh, R. Pandey and S. P. Karna, *J. Phys. Chem. C*, 2015, **119**, 15654–15660.
12 T. Björkman, S. Kurasch, O. Lehtinen, J. Kotakoski, O. V. Yazyev, A. Srivastava, V. Skakalova, J. H. Smet, U. Kaiser and A. V. Krasheninnikov, *Sci. Rep.*, 2013, **3**, 3482.
13 S. He, P. Cavanagh and J. Intriligator, *Nature*, 1996, **383**, 334–337.
14 K. J. Kingma, R. E. Cohen, R. J. Hemley and H.-K. Mao, *Nature*, 1995, **374**, 243–245.
15 D. Andrault, G. Fiquet, F. Guyot and M. Hanfland, *Science*, 1998, **282**, 720–724.
16 D. L. Lakshtanov, S. V. Sinogeikin, K. D. Litasov, V. B. Prakapenka, H. Hellwig, J. Wang, C. Sanches-Valle, J.-P. Perrillat, B. Chen and M. Somayazulu, *Proc. Natl. Acad. Sci. U. S. A.*, 2007, **104**, 13588–13590.
17 J. P. Perdew, K. Burke and M. Ernzerhof, *Phys. Rev. Lett.*, 1996, **77**, 3865.
18 G. Kresse and J. Furthmüller, *Phys. Rev. B: Condens. Matter*, 1996, **54**, 11169.
19 J. Heyd, G. E. Scuseria and M. Ernzerhof, *J. Chem. Phys.*, 2003, **118**, 8207–8215.
20 H. J. Monkhorst and J. D. Pack, *Phys. Rev. B: Solid State*, 1976, **13**, 5188–5192.
21 P. Giannozzi, S. Baroni, N. Bonini, M. Calandra, R. Car, C. Cavazzoni, D. Ceresoli, G. L. Chiarotti, M. Cococcioni, I. Dabo, A. Dal Corso, S. de Gironcoli, S. Fabris, G. Fratesi, R. Gebauer, U. Gerstmann, C. Gougoussis, A. Kokalj, M. Lazzeri, L. Martin-Samos, N. Marzari, F. Mauri, R. Mazzarello, S. Paolini, A. Pasquarello, L. Paulatto, C. Sbraccia, S. Scandolo, G. Sclauzero, A. P. Seitsonen, A. Smogunov, P. Umari and R. M. Wentzcovitch, *J. Phys.: Condens. Matter*, 2009, **21**, 395502.
22 S. Nosé, *J. Chem. Phys.*, 1984, **81**, 511–519.
23 N. Troullier and J. L. Martins, *Phys. Rev. B: Condens. Matter*, 1991, **43**, 8861–8869.
24 P. B. Sorokin, A. G. Kvashnin, Z. Zhu and D. Tománek, *Nano Lett.*, 2014, **14**, 7126–7130.
25 C.-C. Chen, A. Herhold, C. Johnson and A. Alivisatos, *Science*, 1997, **276**, 398–401.
26 A. K. Singh, K. Mathew, H. L. Zhuang and R. G. Hennig, *J. Phys. Chem. Lett.*, 2015, **6**, 1087–1098.
27 S. Grimme, *J. Comput. Chem.*, 2006, **27**, 1787–1799.
28 R. Q. Zhang, A. De Sarkar, T. A. Niehaus and T. Frauenheim, *Phys. Status Solidi B*, 2012, **249**, 401–412.
29 C. Noguera, *J. Phys.: Condens. Matter*, 2000, **12**, R367.
30 J. Fritsch, O. F. Sankey, K. E. Schmidt and J. B. Page, *Phys. Rev. B: Condens. Matter*, 1998, **57**, 15360.
31 M. Lazzeri and F. Mauri, *Phys. Rev. Lett.*, 2003, **90**, 036401.
32 T. L. Weeding, B. Dejong, W. S. Veeman and B. G. Aitken, *Nature*, 1985, **318**, 352–353.
33 S. Zhang, J. Zhou, Q. Wang and P. Jena, *J. Phys. Chem. C*, 2013, **117**, 1064–1070.
34 Y. Ding and Y. Wang, *J. Phys. Chem. C*, 2013, **117**, 18266–18278.
35 E. Cadelano and L. Colombo, *Phys. Rev. B: Condens. Matter*, 2012, **85**, 245434.
36 E. Cadelano, P. L. Palla, S. Giordano and L. Colombo, *Phys. Rev. B: Condens. Matter*, 2010, **82**, 235414.
37 Y. Wang and Y. Ding, *Phys. Status Solodi RRL*, 2013, **7**, 410–413.

38 N. R. Keskar and J. R. Chelikowsky, *Nature*, 1992, **358**, 222–224.
39 J.-W. Jiang and H. S. Park, *Nat. Commun.*, 2014, **5**, 4727.
40 S. Zhang, J. Zhou, Q. Wang, X. Chen, Y. Kawazoe and P. Jena, *Proc. Natl. Acad. Sci. U. S. A.*, 2015, **112**, 2372–2377.
41 W. Tang, E. Sanville and G. Henkelman, *J. Phys.: Condens. Matter*, 2009, **21**, 084204.
42 K. Khoo and S. G. Louie, *Phys. Rev. B: Condens. Matter*, 2004, **69**, 201401.
43 C.-H. Park and S. G. Louie, *Nano Lett.*, 2008, **8**, 2200–2203.
44 Z. Zhang and W. Guo, *Phys. Rev. B: Condens. Matter*, 2008, **77**, 075403.
45 J. Yu and W. Guo, *J. Phys. Chem. Lett.*, 2013, **4**, 1856–1860.
46 A. Ramasubramaniam, D. Naveh and E. Towe, *Phys. Rev. B: Condens. Matter*, 2011, **84**, 205325.